WILEY-VCH

DOI: 10.1002/adfm.201909028
Article type: Full Paper

Non-linear work function tuning of lead-halide perovskites by MXenes with mixed terminations

Alessia Di Vito, Alessandro Pecchia, Matthias Auf der Maur, and Aldo Di Carlo**

A. Di Vito
Department of Electronics Engineering, University of Rome Tor Vergata, Via del Politecnico 1, 00133 Rome, Italy

Dr. A. Pecchia
CNR-ISMN, Via Salaria Km 29.300, 00017 Monterotondo (Rome), Italy
E-mail: alessandro.pecchia@cnr.it

Prof. M. Auf der Maur
Department of Electronics Engineering, University of Rome Tor Vergata, Via del Politecnico 1, 00133 Rome, Italy

Prof. A. Di Carlo
CHOSE - Centre for Hybrid and Organic Solar Energy, Department of Electronics Engineering, University of Rome Tor Vergata, Via del Politecnico 1, 00133 Rome, Italy
CNR-ISM, Via del Fosso del Cavaliere 100, 00133 Rome, Italy
E-mail: aldo.dicarlo@uniroma2.it

Keywords: MXenes, perovskites, work function tuning, DFT calculations, perovskite solar cells

MXenes are a recent family of 2D materials with very interesting electronic properties for device applications. One of such very appealing features is the wide range of work functions shown by these materials, depending on their composition and surface terminations, that can be exploited to adjust band alignments between different material layers. In this work, based on Density Functional Theory calculations, we analyze in detail how mixed terminations of F, OH and/or O affect the work function of Ti_3C_2 MXene, covering the whole phase-space of mixtures. We also analyze the $Ti_3C_2/CH_3NH_3PbI_3$ ($MAPbI_3$) perovskite coupled system for solar cell applications. A strong non-linear behavior is found when varying the relative concentrations of OH, O and F terminations, with the strongest effect of the OH groups in lowering the work function, already at a relative amount of 25%. A surprising minimum work

function is found for relative OH:O fraction of 75:25, explained in terms of the non-linear electronic response in screening the surface dipoles.

1. Introduction

Lead-halide perovskite solar cells (PSC) have gained a key role in the research of 3rd generation renewable energy sources due to their high efficiency and competitive production costs. A great deal of effort is expended worldwide to improving their stability, crystal quality and performance. It has been consolidated that charge transfer at material interfaces, band alignment and energy barriers play fundamental roles in ruling device performance and stability.[1-3] In this context, two-dimensional (2D) materials have been sought as promising interface layers in order to improve PSC electrical properties,[4] due to their good electrical conductivity, mechanical robustness, easy production and solution processability.[5-9] Graphene was one of the first of such 2D materials to be explored in SCs, either in between the transparent conductive oxide (TCO) and the electron transport layer (ETL),[10-12] or to replace TCO.[13] Transition metal di-calchogenides such as MoS_2 have been employed as electron and hole transport inter-layers,[14] both in normal and inverted structures, or as ink-processed material within the perovskite matrix.[15,16] A very appealing feature of 2D materials is the possibility of tuning their chemical and electronic properties by functionalization.[17] For instance, after oxidation via Hammer's method, graphene can be turned into a hydrophilic material for easier solution process. Graphene fluorinated at different concentrations has been employed as work function grading in order to improve electron extraction in inverted architectures.[18]

Recently, MXenes have emerged as a new class of conducting materials that can be incorporated in PSC structures, resulting in a remarkable improvement of device efficiency.[19-21] MXenes are 2D transition metal carbides or nitrides with chemical composition $M_{n+1}X_n$, where M is an early transition metal and X is carbon or nitrogen.[22,23]

They are derived from exfoliation of the $M_{n+1}AX_n$ phases (MAX),[24-28] using hydrofluoric acid removing the A element (usually, IIIA and IVA elements, such as aluminum). As a result of this process the obtained two-dimensional $M_{n+1}X_n$ flakes are spontaneously terminated by F, OH, or O groups.[22] These materials are typically metals, showing a work function variability, depending on the transition metal and the X element.[29] The widest range of work function (WF), though, depends on the termination group, strongly affecting the surface dipole.[30-32] Bare Ti_3C_2 MXene has a WF of 4.5 eV, that can be shifted down to as low as 1.6 eV for OH terminated surfaces or up to 6.25 eV for O termination.[30] This very broad range opens new exciting opportunities for applications. In particular, fine-tuning of the WF allows to tune the vacuum level and obtain appropriate energy level alignment at interfaces, leading to an ideal energy offset between the perovskite active layer and the charge transport layers. This effect was shown in the study of Liu et al.,[32] where MXenes have been used to reduce the Schottky barrier for electron injection with 2D semiconductors. In fact, MXenes have been successfully used in PSCs.[20,21,33] Very recently a thorough study has shown that MXenes can be used to fine tune the band alignment between the perovskite layer and both the ETL and HTL, with a significant improvement of both J_{sc} and V_{oc} as well as the fill factor (FF), resulting in efficiencies that can be improved from 15% to above 20%.[19]

In the present work, density functional theory (DFT) calculations have been performed in order to study the interaction of MXene and perovskite, evidencing a strong non-linear behavior in the interface WF when varying the relative fraction of OH, O and F MXene terminations. A preliminary indication of this non-linearity is found in the study of Schultz et al.,[34] in which it has been shown that the WF of MXenes with mixed terminations could not be simply reproduced by linearly interpolating the WF of purely terminated surfaces. However, the analysis of Schultz et al. has been performed for specific MXene structures obtained at specific values of temperature. Here, the whole phase-space of different MXene surface terminations is considered and the analysis is extended to the MXene/perovskite

interface. Moreover, we quantitatively describe the degree and origin of the non-linearity observed in the WF behavior.

2. Computational Approach

In order to simulate the perovskite/MXenes interaction, we considered a $CH_3NH_3PbI_3$ ($MAPbI_3$) perovskite structure in its high temperature cubic phase and a functionalized $Ti_3C_2T_x$ MXene structure, with the functional termination groups being OH, F or O. From here on, we refer to $Ti_3C_2T_x$ as MXene and to $MAPbI_3$ as perovskite throughout the rest of the text.

The unit cell of the high temperature (>330 K) cubic $MAPbI_3$ has a lattice parameter of $a = 6.2$ Å, as derived by DFT geometry optimization, and contains one $MAPbI_3$ unit cell comprising 12 atoms. The structure of bare Ti_3C_2 consists of five atomic layers with a hexagonal unit cell,[35] where carbon sheets are sandwiched between the Ti sheets (i.e., Ti-C-Ti-C-Ti) alternating as an fcc-like close packing. Then, the functionalized MXenes are obtained by assuming both surfaces completely terminated by OH, F or O groups placed at the hollow sites, that have been found energetically more stable.[36]

We consider $MAPbI_3$ perovskite exposing the PbI_2 terminated surface. This is the recommended choice for $MAPbI_3$ surface simulations,[37] as several experiments indicate a slight iodine deficiency in the $MAPbI_3$ surface composition.[38] In the study of Agresti et al.,[19] the open surface exposing MA-Iodine was considered because this surface seems to naturally bind spiroOmetad or PCBM hole transport layers, but computationally gives a lower ionization energy (4.7 eV vs 5.8 eV), where 5.5 eV is an accepted experimental value.[19] Due to the pronounced lattice mismatch between $MAPbI_3$ and MXene and cubic vs hexagonal symmetries, we used large commensurate supercells in order to minimize strain or artificial distortions at the interface. The slab contains 162 $MAPbI_3$ atoms and 196 (252) Ti_3C_2O/F (Ti_3C_2OH) atoms, corresponding to 1×6×2 perovskite unit cells and 2×14×1 MXenes unit

cells. Hence, simulations are performed using a slab configuration with approximately 12.4 Å of $MAPbI_3$, 9 Å of $Ti_3C_2T_x$ and 20 Å of vacuum. In this way the lattice mismatch at the interface is reduced to less than 1%.

First-principles calculations based on DFT within the local density approximation (LDA) are performed using the Quantum Espresso package.[39] The DFT-LDA approach was previously applied for the calculation of functionalized MXenes work functions and the validation using the generalized gradient approximation (GGA) is discussed below. Scalar-relativistic PAW pseudopotentials are employed,[40] with the exchange-correlation (XC) functional parameterized by Perdew-Zunger.[41] A Γ-centered 8×1×1 Monkhorst-Pack k-point grid was employed,[42] with 50 Ry of cutoff energy and a self-consistent energy tolerance of 10^{-2} eV. The reliability of the LDA approximation has been tested performing preliminary calculations of the bare and terminated Ti_3C_2 work function using the GGA of Perdew-Burke-Ernzerhof (PBE) for the XC functional.[43] The results are shown in Figure S1 of Supporting Material (SM) and compared with the reference DFT-GGA study of Khazaei et al..[30]

All the structures considered in this work are fully relaxed under periodic boundary conditions until the residual force on each atom is below 10^{-2} eV/Å and the total energy correction is below 10^{-2} eV, with a Γ-centered 4×1×1 Monkhorst-Pack k-point grid.

The optimized slab structures are shown in Figure S2 of SM. The most relevant feature of the MXenes/perovskite interface is a slight distortion of the surface PbI_2 layer in contact with MXenes, particularly evident for the O terminated structure shown in **Figure 1**. In general, however, we do not observe a large distortion of the geometries.

3. Results and Discussion

In order to understand the behavior of the MXene/$MAPbI_3$ coupled system, we first analyze the WF of MXene alone, for different termination fractions. We take the average over three random samples for each surface composition. OH, O and F terminations are distributed at

random on the MXene surface and the symmetry between top and bottom surfaces is preserved. The WF derived for different random configurations varies by less than 50 meV, that is approximately 1% of the considered range of WF values.

The computations are performed by looking at the difference of the electrostatic potential in the vacuum and the electron Fermi energy.[44] Typical plots of the plane-averaged electrostatic potential used for these calculations are shown in Figure S3 of the SM. The collected results are reported in **Figure 2**, showing an interpolating quadratic function that covers the whole phase-space of relative F:OH:O concentrations. In the same Figure, we have added the measured (black star)[19] WF for the mixture F:OH:O distributed at random with relative amounts 62:25:13, as determined by XPS measurements.[19] The agreement between theoretical (3.75 eV) and experimental (3.69 eV) values is very good, differing by less than 2%.

Notably, the trends reported in Figure 2 are highly non-linear. In particular, we find that both the OH:F and OH:O compositions exhibit a minimum in the WF for the relative fraction of 75% OH, with a deeper minimum along the OH:O line. This minimum is also confirmed by GGA calculations (see Figure S5 of SM and the related discussion). This is a remarkable and unexpected feature, since the WF is expected to increase monotonically when the density of OH sites is decreased.

In order to understand this effect, we have looked more in detail at the behavior of the calculated charge densities and surface dipoles. It is not difficult to verify (see Section 2 of SM) that the plane averaged charge density, $\rho(z)$, fulfills a Poisson equation for the plane averaged potential along the direction z, orthogonal to the slab. It is also easy to see that any potential variation between interior and vacuum is related to a variation of dipole moment, $\Delta\varphi = -\Delta p/\epsilon_0 = -1/\epsilon_0 \int_0^\infty \Delta\rho(z) z dz$, where we have defined the middle of the MXene slab at $z = 0$. This potential variation directly translates into a variation of WF under the

assumption that the Fermi level does not shift with respect to the potential inside the slab, which is always true for sufficiently thick slabs. Hence, the WF variation is $\Delta\Phi \sim -\Delta p$.

A rationale for the decrease of WF for OH terminated MXene is that OH groups have a large positive dipole originating from a fractional electron transfer from H to O. Similarly, in O terminated structures there is an opposite polarization of the surface. In general, the WF change could also depend on possible atomic relaxations of Ti and C atoms,[44] but this is found of secondary importance, giving WF variations of less than 100 meV.

In the following we consider more in detail the variation of WF when varying the OH:O relative fraction. The variation of charge density between terminated and bare MXene, $\Delta\rho(z) = \rho^{tot}(z) - \rho^{sub}(z)$, can be expressed in terms of the corresponding contributions,

$$\rho^{sub}(z) = \sum_{i\in Ti,C} Z_i \delta(z - z_i) - n^{sub}(z) \quad (1)$$

$$\rho^{tot}(z) = \sum_{i\in Ti,C,O,H} Z_i \delta(z - z_i) - n^{tot}(z) \quad (2)$$

where Z_i is the ionic charge and z_i the ion position, $n^{sub}(z)$ is the electronic density in the substrate alone and $n^{tot}(z)$ is the electronic density of the coupled system. Since the ionic positions of the substrate are kept frozen in the two calculations, $\Delta\rho(z)$ simplifies into,

$$\Delta\rho(z) = \sum_{i\in O,H} Z_i \delta(z - z_i) - n^{tot}(z) + n^{sub}(z) \quad (3)$$

By adding and subtracting the electronic density of the terminal layer, $n^{OH/O}(z)$, we can split $\Delta\rho$ into two contributions. The first one is the charge density of the isolated terminal groups, $\rho^{OH/O}(z) = \sum_{i\in O,H} Z_i \delta(z - z_i) - n^{OH/O}(z)$, and the other is the rearrangement of the

electronic density, $\Delta n(z) = n^{tot}(z) - \left[n^{sub}(z) + n^{OH/O}(z)\right]$. From these charge densities it is possible to compute two corresponding contributions to the surface dipole,

$$p^{OH/O} = 1/\epsilon_0 \int_0^\infty \Delta\rho^{OH/O}(z) z dz \quad (4)$$

$$p^{n} = -1/\epsilon_0 \int_0^\infty \Delta n(z) z dz. \quad (5)$$

The variation of the electronic density, $\Delta n(z)$, for the 100% OH and for the 75% OH 25% O terminated Ti_3C_2 surfaces, are shown in **Figure 3a** and **3b**, respectively. We can see that in both cases there is a depletion of electron charge in the Ti_3C_2 surface layer and an increased electron charge in the O layer. This indicates a charge transfer from the Ti_3C_2 surface to the OH/O terminal groups, in agreement with the difference in electronegativity between titanium and oxygen. Notably, for the 100% OH covered surface Δn exhibits an increased electron charge density in the tail region away from the OH layer, as highlighted by the shaded areas in Figure 3a. This is the result of the electronic cloud screening the OH dipoles. In fact, in this case, the total dipole of the OH layer is $p^{OH} = 6.5\ e$Å, whereas $p^{n} = -3.9\ e$Å, giving a net interface dipole of $\Delta p = 2.6\ e$Å. The electronic tail seen in Figure 3a practically disappears in Figure 3b, for the 75:25 mixed surface, where the adsorbate dipole decreases to $p^{OH/O} = 5.8\ e$Å. This effect strongly reduces the magnitude of $p^{n} = -1.9\ e$Å, resulting in a larger net dipole variation of $\Delta p = 3.9\ e$Å and a lower WF. In practice the non-linear behavior of the electronic screening explains the lower WF in the case of mix passivation. This non-linearity can also be seen in **Figure 4**, reporting the behavior of $p^{OH/O}$, p^{n} and Δp when varying the relative fraction of OH:O terminal sites. The termination dipole, $p^{OH/O}$, decreases almost linearly when the OH fraction decreases, showing a moderate deviation from linearity only at maximum coverage, when dipole-dipole interactions become relevant. On the other hand, the

dipole associated to the electronic cloud turns strongly negative for 100% OH termination, leading to a maximum in Δp for 75:25 relative fractions.

We now consider the interaction of MXene and $MAPbI_3$. The x-y plane averaged electrostatic potential of the $MAPbI_3/Ti_3C_2OH$, $MAPbI_3/Ti_3C_2F$ and $MAPbI_3/Ti_3C_2O$ slabs are plotted along the z direction perpendicular to the interface in Figure S3 of SM. The Fermi energy is set to zero, so that the vacuum potential level corresponds to the WF value. Specifically, the WF of the perovskite/MXene interface is labeled by Φ_1 and is derived considering the vacuum level in contact with the MXene surface.[45] On the other hand, the $MAPbI_3$ WF is represented by Φ_2 and is obtained from the vacuum level at the vacuum/perovskite interface. The values of Φ_1 and Φ_2 for the considered MXene terminal groups are listed in **Table 1**.

The WF of the perovskite/MXene interface is affected by the nature of the MXene surface termination. The Φ_1 value obtained for the OH terminated MXene structure is strongly reduced with respect to the bulk $MAPbI_3$ WF, $\Phi_0 = 5.1\ eV$. On the contrary, the O terminated MXene induces an increment of Φ_1 with respect to the undoped perovskite. For the $MAPbI_3/Ti_3C_2F$ interface, the WF slightly deviates from Φ_0. The origin of the interface WF tuning caused by different terminal groups is the electrostatic interaction between MXene and perovskite. The vacuum potential slopes observed in Figure S3 indicate the formation of an electrostatic dipole at the perovskite/MXene interface, due to the charge redistribution. Notably, the interface dipole is more pronounced for the $MAPbI_3/Ti_3C_2OH$ system. Moreover, for the OH terminated MXene configuration, the Fermi energy is shifted within the conduction band of $MAPbI_3$, as depicted in Figure S6 and S7 of SM, where the perovskite projected density of states is reported. Here, the $MAPbI_3$ valence band maximum is set to zero and the band gap is represented by the gray area. The O functionalized MXene has the opposite effect. As observed in Figure S3, the charge transfer at the $MAPbI_3/Ti_3C_2O$ interface induces the formation of an interface dipole with opposite direction with respect to

$MAPbI_3/Ti_3C_2OH$. Furthermore, it can be seen in Figure S6 that the Fermi level is down-shifted with respect to the $MAPbI_3$ band edges, for the O terminated Ti_3C_2.

In principle, the value of Φ_2 should correspond to the bulk $MAPbI_3$ WF, $\Phi_0 = 5.1\ eV$. However, the thickness of the perovskite layer considered in our simulations (i.e., 12.4 Å) is not sufficient to recover the bulk configuration of $MAPbI_3$. As a matter of fact, the Fermi energy, that is located at mid-gap for the undoped bulk perovskite, results up-shifted for the $MAPbI_3/Ti_3C_2OH$ and $MAPbI_3/Ti_3C_2F$ systems, as it can be observed in Figure S6 and S7. The up-shift of the Fermi level corresponds to the reduction of the WF Φ_2 with respect to the expected bulk value Φ_0. On the other hand, the Fermi energy for the $MAPbI_3/Ti_3C_2O$ structure is shifted within the valence band of $MAPbI_3$, as shown in Figure S6, and the down-shift of the Fermi level corresponds to the increase of Φ_2 with respect to Φ_0. The entity of the Fermi energy shift, corresponding to the deviation of the Φ_2 value with respect to Φ_0 (i.e., $\Phi_0 - \Phi_2 = \Delta E_f$), is listed in Table 1 for all the considered MXene functional groups.

The band profiles derived from the obtained results are schematically sketched in **Figure 5a**, **5b** and **5c** for the $MAPbI_3/Ti_3C_2OH$, $MAPbI_3/Ti_3C_2F$ and $MAPbI_3/Ti_3C_2O$ interfaces, respectively.

The WF reduction induced by the OH terminated MXene surface is much more pronounced than the WF increase induced by O terminations. Thus, assuming a mixture of the different terminations, we expect a non-linear WF trend, with the overall effect of MXene adsorption on perovskite generally leading to a reduction of the interface WF.

In order to investigate this effect, we studied the behavior of Φ_1 when the fraction of OH, O and F terminal groups is varied. We considered a random configuration where the different sites are distributed at random on the MXene surface. We assume completely functionalized MXene surfaces and the symmetry between top and bottom surfaces is preserved. The obtained results are reported in **Figure 6**. We can see that Φ_1 exhibits a pronounced non-

linear behavior when the fraction of different terminal sites is varied. In fact, the WF of MXene itself is affected in a non-linear fashion by mixed surface terminations, as discussed for Figure 2 and in agreement with previous studies.[34] In particular, we can observe in Figure 6 the presence of a minimum WF value in both the OH/O and OH/F trends when the relative fraction of OH terminations is 75%, as pointed out for the MXene WF shown in Figure 2. The behavior of Φ_2 for mixed surface terminations is reported in Figure S8 of SM for completeness.

4. Conclusion

To summarize, we studied the perovskite/MXene interface using a DFT approach, where the MXene surfaces are terminated by F, OH and/or O functional groups. We found that the charge redistribution at the interface induces the formation of an electrostatic dipole that affects the interface WF value, depending on the nature of the MXene surface terminations. Notably, the interface WF exhibits a highly non-linear behavior when the fraction of OH, O and F terminal groups is varied. This non-linearity is also found in the response of MXene itself for a mixture of OH, O and F functional groups. The WF of MXene can be well interpolated in the whole phase-space of different terminations by a quadratic function. Interestingly, we found that both the OH/O and OH/F trends present a minimum WF value when the fraction of OH sites is 75%. We analyzed and sized the degree and origin of the WF non-linearity observed in both the MXene and Perovskite/MXene systems for mixed surface terminations, as originating from the non-linear response of the electronic density of the system to the termination dipoles.

Supporting Information

Supporting Information is available from the Wiley Online Library or from the author.

Received: ((will be filled in by the editorial staff))
Revised: ((will be filled in by the editorial staff))
Published online: ((will be filled in by the editorial staff))

References

[1] P. Schulz, *ACS Energy Lett.* **2018**, *3*, 1287–1293.

[2] S. Wang, T. Sakurai, W. Wen, Y. Qi, *Adv. Mater. Interfaces* **2018**, *5*, 1800260.

[3] S. Olthof, *APL Mater.* **2016**, *4*, 091502.

[4] P. You, G. Tang, F. Yan, *Mater. Today Energy* **2019**, *11*, 128 – 158.

[5] W. H. Lee, Y. D. Park, *Adv. Mater. Interfaces* **2018**, *5*, 1700316.

[6] D. Akinwande, C. J. Brennan, J. Scott Bunch, P. Egberts, J. R. Felts, H. Gao, R. Huang, J.-S. Kim, T. Li, Y. Li, K. M. Liechti, N. Lu, H. S. Park, E. J. Reed, P. Wang, B. I. Yakobson, T. Zhang, Y.-W. Zhang, Y. Zhou, Y. Zhu, *Extreme Mech. Lett.* **2017**, *13*, 42–77.

[7] X. Bao, Q. Ou, Z.-Q. Xu, Y. Zhang, Q. Bao, H. Zhang, *Adv. Mater. Technologies* **2018**, *3*, 1800072.

[8] Y. Yao, Z. Lin, Z. Li, X. Song, K.-S. Moon, C.-P. Wong, *J. Mater. Chem.* **2012**, *22*, 13494–13499.

[9] X. Cai, Y. Luo, B. Liu, H.-M. Cheng, *Chem. Soc. Rev.* **2018**, *47*, 6224–6266.

[10] Z. Zhu, J. Ma, Z. Wang, C. Mu, Z. Fan, L. Du, Y. Bai, L. Fan, H. Yan, D. L. Phillips, *J. Am. Chem. Soc.* **2014**, *136*, 3760–3763.

[11] K. T. Cho, G. Grancini, Y. Lee, D. Konios, S. Paek, E. Kymakis, M. K. Nazeeruddin, *ChemSusChem* **2016**, *9*, 3040–3044.

[12] A. Agresti, S. Pescetelli, B. Taheri, A. E. Del Rio Castillo, L. Cina, F. Bonaccorso, A. Di Carlo, *ChemSusChem* **2016**, *9*, 2609–2619.

[13] H. Sung, N. Ahn, M. S. Jang, J.-K. Lee, H. Yoon, N.-G. Park, M. Choi, *Adv. Energy Mater.* **2015**, *6*, n/a.

[14] R. Singh, A. Giri, M. Pal, K. Thiyagarajan, J. Kwak, J.-J. Lee, U. Jeong, K. J. Cho, *Mater. Chem. A* **2019**, *7*, 7151–7158.

[15] L. Najafi, B. Taheri, B. Martin-Garcia, S. Bellani, D. Di Girolamo, A. Agresti, R. Oropesa-Nunez, S. Pescetelli, L. Vesce, E. Calabro, M. Prato, A. E. Del Rio Castillo, A. Di Carlo, F. Bonaccorso, *ACS Nano* **2018**, *12*, 10736–10754.

[16] P. O'Keeffe, D. Catone, A. Paladini, F. Toschi, S. Turchini, L. Avaldi, F. Martelli, A. Agresti, S. Pescetelli, A. E. Del Rio Castillo, F. Bonaccorso, A. Di Carlo, *Nano Lett.* **2019**, *19*, 684–691.

[17] D. Konios, G. Kakavelakis, C. Petridis, K. Savva, E. Stratakis, E. Kymakis, *J. Mater. Chem. A* **2016**, *4*, 1612–1623.

[18] J.-H. Yu, C.-H. Lee, H.-I. Joh, J.-S. Yeo, S.-I. Na, *Nanoscale* **2017**, *9*, 17167–17173.

[19] A. Agresti, A. Pazniak, S. Pescetelli, A. Di Vito, D. Rossi, A. Pecchia, M. Auf der Maur, A. Liedl, R. Larciprete, D. V. Kuznetsov, D. Saranin, A. Di Carlo, *Nat. Mater.* **2019**, *18*, 1228–1234.

[20] Z. Guo, L. Gao, Z. Xu, S. Teo, C. Zhang, Y. Kamata, S. Hayase, T. Ma, *Small* **2018**, *14*, 1802738.

[21] L. Yang, Y. Dall'Agnese, K. Hantanasirisakul, C. E. Shuck, K. Maleski, M. Alhabeb, G. Chen, Y. Gao, Y. Sanehira, A. K. Jena, L. Shen, C. Dall'Agnese, X.-F. Wang, Y. Gogotsi, T.J. Miyasaka, *Mater. Chem. A* **2019**, *7*, 5635–5642.

[22] M. Naguib, M. Kurtoglu, V. Presser, J. Lu, J. Niu, M. Heon, L. Hultman, Y. Gogotsi, M. W. Barsoum, *Adv. Mater.* **2011**, *23*, 4248–4253.

[23] M. Naguib, O. Mashtalir, J. Carle, V. Presser, J. Lu, L. Hultman, Y. Gogotsi, M. W. Barsoum, *ACS Nano* **2012**, *6*, 1322–1331.

[24] M. Khazaei, M. Arai, T. Sasaki, M. Estili, Y. Sakka, *J. Phys.-Condens. Mat.* **2014**, *26*, 505503.

[25] M. W. Barsoum, *Prog. Solid State Ch.* **2000**, *28*, 201–281.

[26] Z. Sun, *Int. Mater. Rev.* **2011**, *56*, 143–166.

[27] M. Cover, O. Warschkow, M. Bilek, D. McKenzie, *J. Phys.-Condens. Mat.* **2009**, *21*, 305403.

[28] M. Khazaei, M. Arai, T. Sasaki, M. Estili, Y. Sakka, *Sci. Technol. Adv. Mat.* **2014**, *15*, 014208.

[29] M. Khazaei, A. Ranjbar, M. Arai, T. Sasaki, S. Yunoki, *J. Mater. Chem. C* **2017**, *5*, 2488–2503.

[30] M. Khazaei, M. Arai, T. Sasaki, A. Ranjbar, Y. Liang, S. Yunoki, *Phys. Rev. B* **2015**, *92*, 075411.

[31] T. Hu, Z. Li, M. Hu, J. Wang, Q. Hu, Q. Li, X. Wang, *J. Phys. Chem. C* **2017**, *121*, 19254–19261.

[32] Y. Liu, H. Xiao, W. A. Goddard III, *J. Am. Chem. Soc.* **2016**, *138*, 15853–15856.

[33] L. Yang, C. Dall'Agnese, Y. Dall'Agnese, G. Chen, Y. Gao, Y. Sanehira, A. K. Jena, X.-F. Wang, Y. Gogotsi, T. Miyasaka, *Adv. Funct. Mater.* **2019**, *29*, 46, 1905694.

[34] T. Schultz, N. C. Frey, K. Hantanasirisakul, S. Park, S. J. May, V. B. Shenoy, Y. Gogotsi, N. Koch, *Chem. Mater.* **2019**, *31*, 17, 6590-6597.

[35] I. Shein, A. Ivanovskii, *Comp. Mater. Sci.* **2012**, *65*, 104–114.

[36] A. N. Enyashin, A. L. Ivanovskii, *J. Phys. Chem. C* **2013**, *117*, 13637–13643.

[37] G. Volonakis, F. Giustino, *J. Phys. Chem. Lett.* **2015**, *6*, 2496–2502.

[38] R. Lindblad, D. Bi, B.-W. Park, J. Oscarsson, M. Gorgoi, H. Siegbahn, M. Odelius, E. M. Johansson, H. Rensmo, *J. Phys. Chem. Lett.* **2014**, *5*, 648–653.

[39] P. Giannozzi, S. Baroni, N. Bonini, M. Calandra, R. Car, C. Cavazzoni, D. Ceresoli, G. L. Chiarotti, M. Cococcioni, I. Dabo, A. Dal Corso, S. de Gironcoli, S. Fabris, G. Fratesi, R. Gebauer, U. Gerstmann, C. Gougoussis, A. Kokalj, M. Lazzeri, L. Martin-Samos, N. Marzari, F. Mauri, R. Mazzarello, S. Paolini, A. Pasquarello, L. Paulatto, C. Sbraccia, S. Scandolo, G. Sclauzero, A. P. Seitsonen, A. Smogunov, P. Umari, R. M. Wentzcovitch, *J. Phys.-Condens. Mat.* **2009**, *21*, 395502.

[40] Quantum Espresso, www.quantum-espresso.org/pseudopotentials.

[41] J. Perdew, *Phys. Rev. B* **1981**, *23*, 5048.

[42] H. J. Monkhorst, J. D. Pack, *Phys. Rev. B* **1976**, *13*, 5188.

[43] J. P. Perdew, K. Burke, M. Ernzerhof, *Phys. Rev. Lett.* **1996**, *77*, 3865.

[44] T. Leung, C. Kao, W. Su, Y. Feng, C. Chan, *Phys. Rev. B* **2003**, *68*, 195408.

[45] "Oxide ultra–thin films on metals", U. Martinez Pozzoni, *Ph.D. dissertation*, University of Milano Bicocca, **2008/2009**, pag. 29.

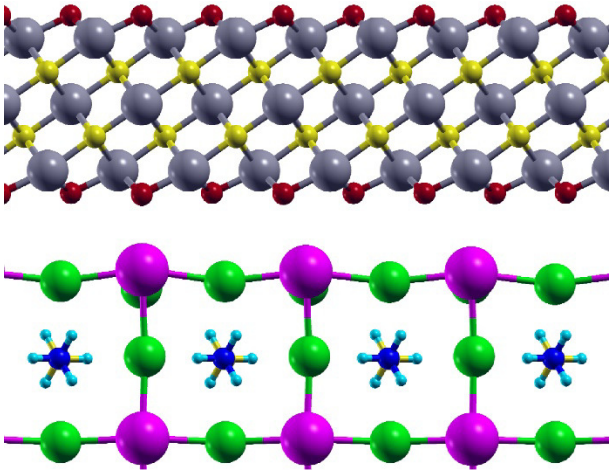

Figure 1. Side view of the simulated $MAPbI_3/Ti_3C_2O$ interface. Grey, yellow, red, cyan, magenta, green and blue spheres represent Ti, C, O, H, Pb, I and N atoms, respectively.

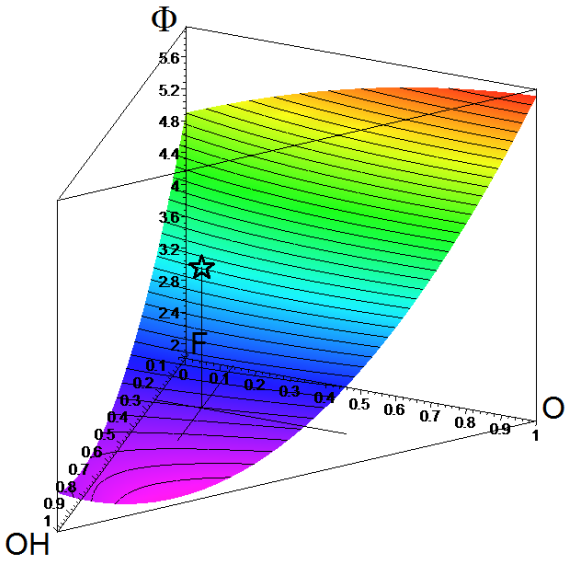

Figure 2. Calculated WF when varying the relative fraction of OH, O and F terminal groups. The plot shows an interpolating quadratic function of the actual calculated data (reported in Figure S4 of SM). The star marks a measured value.[19]

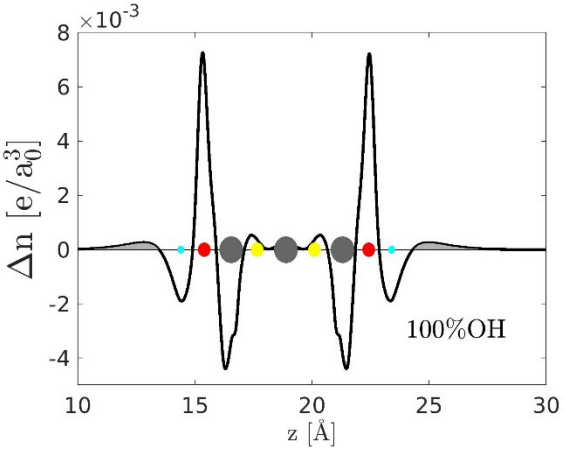

a)

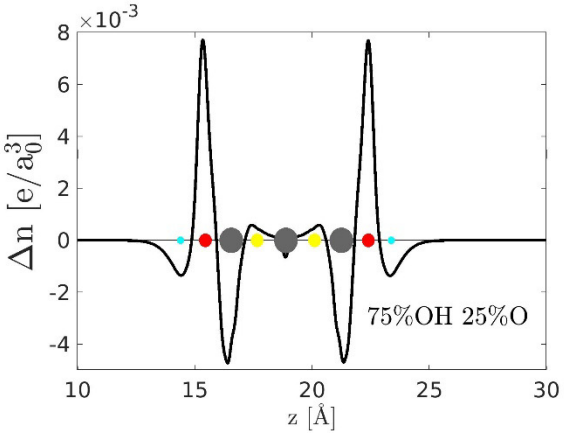

b)

Figure 3. Change in *xy* plane averaged electron charge density as a function of *z* induced by a) 100% OH and b) 75% OH 25%O terminations on Ti_3C_2 MXene surface. Gray, yellow, red and cyan spheres represent Ti, C, O and H atoms, respectively.

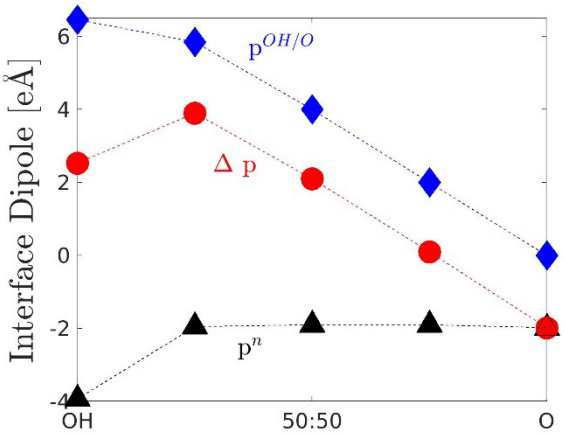

Figure 4. Adsorbate contribution $p^{OH/O}$ (blue data) and electronic rearrangement contribution p^n (black data) to the total interface dipole Δp (red data) for OH/O terminated Ti_3C_2 when the relative amount of OH groups is varied from 100% to 0%.

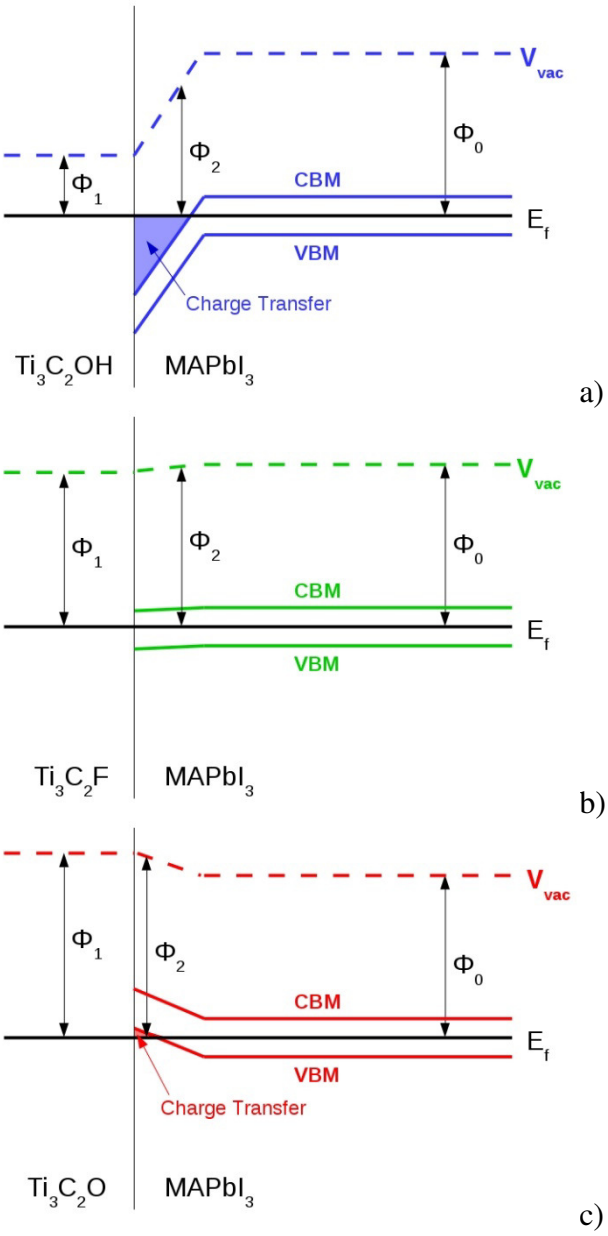

Figure 5. Schematic representation of the band alignment at the a) $MAPbI_3/Ti_3C_2OH$, b) $MAPbI_3/Ti_3C_2F$ and c) $MAPbI_3/Ti_3C_2O$ interfaces.

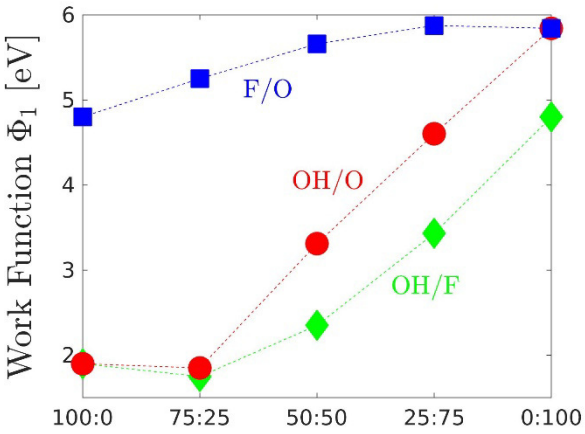

Figure 6. Work function values Φ_1 derived for a mixture of OH, O and F MXene surface terminations at the interface with perovskite.

Table 1. Work function values of the perovskite/MXene interface (Φ_1) and of $MAPbI_3$ perovskite (Φ_2) for all the considered MXene terminal groups. The entity of the Fermi energy shift is also reported. The work function of bulk $MAPbI_3$ is labeled by $\Phi_0 = 5.1\ eV$.

	$MAPbI_3 + Ti_3C_2OH$	$MAPbI_3 + Ti_3C_2F$	$MAPbI_3 + Ti_3C_2O$
Φ_1 [eV]	1.9	4.8	5.8
Φ_2 [eV]	4.2	5.0	5.7
E_f shift (Φ_0-Φ_2) [eV]	0.9 (up-shift)	0.1 (up-shift)	-0.6 (down-shift)

TOC Info and image

We study how F, OH and O mix terminations affect the work function of the Ti_3C_2/$MAPbI_3$ interface, covering the whole phase-space of mixtures and highlighting the mechanism of strong non-linear behaviors. Using first-principles calculations, we describe and size the degree and origin of the work function non-linearity, due to the non-linear response of the electronic density of the system to the termination dipoles.

Keyword MXenes, perovskites, work function tuning, DFT calculations, perovskite solar cells

A. Di Vito, A. Pecchia*, M. Auf der Maur, and A. Di Carlo*

Non-linear work function tuning of lead-halide perovskites by MXenes with mixed terminations

ToC figure (55 mm broad × 50 mm high)